Editors' Suggestion Featured in Physics

Invisible Anchors Trap Particles in Branching Junctions

David Oettinger,[1] Jesse T. Ault,[2] Howard A. Stone,[3] and George Haller[1,*]
[1]*Institute for Mechanical Systems, Department of Mechanical and Process Engineering, ETH Zürich, Leonhardstrasse 21, 8092 Zürich, Switzerland*
[2]*Computational Sciences and Engineering Division, Oak Ridge National Laboratory, Oak Ridge, Tennessee 37831, USA*
[3]*Department of Mechanical and Aerospace Engineering, Princeton University, Princeton, New Jersey 08544, USA*

(Received 6 January 2018; published 3 August 2018)

We combine numerical simulations and an analytic approach to show that the capture of finite, inertial particles during flow in branching junctions is due to invisible, anchor-shaped three-dimensional flow structures. These Reynolds-number-dependent anchors define trapping regions that confine particles to the junction. For a wide range of Stokes numbers, these structures occupy a large part of the flow domain. For flow in a V-shaped junction, at a critical Stokes number, we observe a topological transition due to the merger of two anchors into one. From a stability analysis, we identify the parameter region of particle sizes and densities where capture due to anchors occurs.

DOI: 10.1103/PhysRevLett.121.054502

Branching junctions are building blocks of pipe flow networks that are common in industrial applications [1] and in the arterial system [2]. Because of their simple geometry, one anticipates straightforward fluid behavior in these configurations for moderate flow velocities. In particular, during pumping of a particle-laden fluid into the inlet of a branching junction [Fig. 1(a)], it is natural to expect that both the fluid and the particles will exit through the two outlets. Recent observations, however, reveal the possibility that particles with density smaller than the continuous phase can become trapped in the junction indefinitely [3]. The capture leads to the formation of large particle clouds at the junction. This phenomenon occurs for a significant range of large but laminar flow Reynolds numbers, for several types of particles, and for various junction angles [3,4].

Investigations of the fluid velocity field link the capture mechanism to flow reversal caused by bubble-type vortex breakdown structures near the junction [3,4,6]. The geometry and stability of these vortical structures strongly depend on the Reynolds number and the junction angle [6,7]. While these flow features give strong indications of trapping, here we focus on the fluid-particle interactions, investigating the dynamics of individual inertial particles. Thus, we answer detailed questions about the capture mechanism, such as: How large are the particle-trapping regions? How do particles accumulate within these trapping regions? What properties of the particles and flow influence the trapping?

We consider an experiment with hollow glass beads, less dense than the continuous phase, in a stationary flow of water through a T junction (see Ref. [4] for experimental details). The Reynolds number is $\mathrm{Re} = (\bar{u}L/\nu) = 277$, where $\bar{u}$ is the average inlet flow speed, L is the side length of the square channel, and ν is the kinematic viscosity. Experiments show that a number of particles exit the junction [see Fig. 1(a) and Ref. [5]]. Such particle paths lead either directly to an outlet or show brief recirculation near the vortices in the lower arms of the junction.

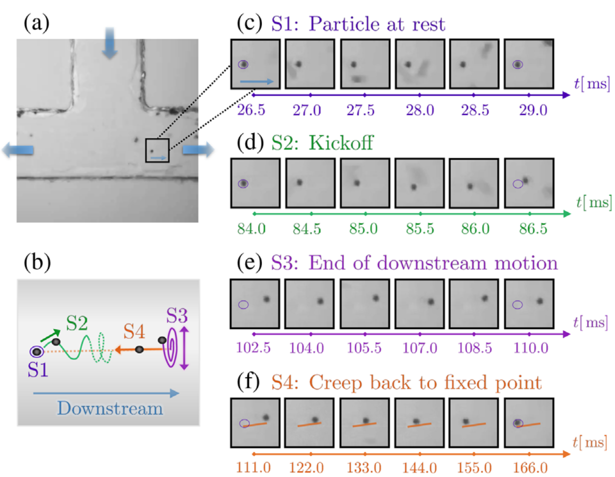

FIG. 1. Analysis of a T-junction experiment with hollow glass beads in a steady flow of water (Re = 277; cf. the video in the Supplemental Material [5]). The density of the beads is $\rho_p = 0.15\rho_f$, where ρ_f is the density of water. (a) Time-lapse image, with arrows marking the inlet (top) and two outlets (left, right). Beads are released at the inlet and exit through one of the outlets. The spiraling of some bead paths (dark gray curves) is due to vortex breakdown in the junction arms. The black box marks the subregion shown in (c)–(f). (b) Illustration of the sequences $S1$–$S4$ shown in (c)–(f). (c) A particle is at rest at a fixed point, while other particles pass by quickly. (d) The particle is displaced by another particle and begins to move downstream. (e) After spiraling downstream, the particle stops its downstream motion and shows damped oscillations perpendicular to the downstream direction. (f) The particle slowly creeps back to its starting position along a line (orange).

As shown in Figs. 1(a) and 1(c), however, we find a single particle at rest within the right vortical region. This particle remains fixed until it is displaced by another particle [Fig. 1(d)]. After briefly moving in the downstream direction, the particle develops rapid spiraling and stops its downstream motion [Fig. 1(e)]. The particle then slowly creeps back to its original spot [Fig. 1(f)]. We summarize the four sequences, $S1$–$S4$, in Fig. 1(b). The observations suggest that the particle dynamics share important similarities with the dynamics of the fluid: First, one of the fixed points known for the fluid phase (cf. Ref. [4]) is preserved and becomes attracting for the particles. Second, particle trajectories resemble streamlines observed in bubble-type vortex breakdown [3,4,6].

We consider particles as small—but finite—noninteracting spheres and choose two representative pipe geometries, a T junction at Re = 320, and a V-shaped junction at an angle of 70° and Re = 230. Rescaling lengths by L, velocities by $\bar{u}$, and time by $(L/\bar{u})$, we model the particle motion by the dimensionless inertial equation (cf. Refs. [5,8–11])

$$\dot{\boldsymbol{x}} = \boldsymbol{v} = \boldsymbol{u} + \varepsilon \frac{D\boldsymbol{u}}{Dt}. \tag{1}$$

Here, $\boldsymbol{x} = (x, y, z)$ is the particle position, the dot denotes the time derivative, $\boldsymbol{v} = \boldsymbol{v}(\boldsymbol{x}, t)$ is the particle velocity, $(D/Dt) = \partial_t + (\boldsymbol{u} \cdot \boldsymbol{\nabla})$ is the material derivative, and $\boldsymbol{u}$ is the fluid velocity field. The small parameter ε in Eq. (1) is given by

$$\varepsilon = \tau(\beta - 1) = \mathrm{St}(1 - \rho) = \frac{2}{9} a^2 \mathrm{Re}(1 - \rho), \tag{2}$$

where $\beta = 3/(1 + 2\rho)$ depends on the ratio ρ between the densities ρ_p of the particles and ρ_f of the fluid, $\rho = \rho_p/\rho_f$, and τ is the dimensionless Stokes time. In terms of the dimensionless particle radius a and Stokes number $\mathrm{St} = \frac{2}{9} a^2 \mathrm{Re}$, we have $\tau = (3/2\beta)\mathrm{St}$. Equation (1) was also obtained by various authors for specific planar steady flows via formal asymptotics [8–10]. Here, we rely on the results of Ref. [11], who obtained this equation from an exact slow-manifold reduction applicable to three-dimensional unsteady flows.

For the fluid velocity field $\boldsymbol{u}$ required by Eq. (1), we use a finite-volume solver from the OpenFOAM library [12] and obtain steady solutions to the three-dimensional, incompressible Navier-Stokes equations (see Ref. [6] for details). As in the experiments, we consider hollow glass beads ($\rho = 0.15$, $5 \times 10^{-4} \lesssim a \lesssim 7 \times 10^{-2}$) and gas bubbles ($\rho = 10^{-3}$, $5 \times 10^{-4} \lesssim a \lesssim 2.5 \times 10^{-2}$) in water [3,4].

Equation (1) allows us to study the accumulation and dispersion of particles over time using the compressible velocity field $\boldsymbol{v}$, which differs from the underlying incompressible fluid velocity field $\boldsymbol{u}$ by a small $O(\varepsilon)$ perturbation. This is consistent with our experimental observations that a fixed point for the particles exists, and that particle trajectories are similar to the known streamlines.

We now investigate the regions within the flow that lead to particle trapping. We define a trapping region (TR) as the largest subdomain of the flow such that, for a fixed ε, particles released within the TR remain inside the TR at all times. To guarantee trapping, a TR must not intersect any of the junction outlets. By definition, therefore, the boundary of a TR is an invariant manifold of Eq. (1). That is, for a fixed ε, particles cannot cross the surface boundary of a TR. Such a surface, therefore, divides the flow domain into an interior region, in which particles are trapped, and an exterior region, from which particles leave the junction.

We choose the representative parameter value $\varepsilon = 0.05$, corresponding to hollow glass beads of radii near the average of $a = 3 \times 10^{-2}$ in the experiments [4]. From the numerically computed velocity field $\boldsymbol{v}$ (1), we identify four fixed points $P_{1,2,3,4}$ in the T-junction flow at Re = 320 [Fig. 2(b)]. Similar fixed points exist in the V-junction flow at Re = 230 [Fig. 2(c)]. With our investigations of representative trajectories suggesting that $P_{1,2,3,4}$ are the primary capture locations as $t \to \infty$ (cf. the Supplemental Material [5], Fig. S1), we compute the domains of attraction of $P_{1,2,3,4}$. Our results (Fig. 2) show that these domains do not intersect with the outlets and hence define TRs. Particles released within a TR accumulate at $P_{1,2,3,4}$ and remain trapped in the junction forever. Specifically, in the T junction at Re = 320 [Figs. 2(a) and 2(b)], both $P_{1,2}$ and $P_{3,4}$ define two separate TRs that touch at $x = 0$, $z = 0$.

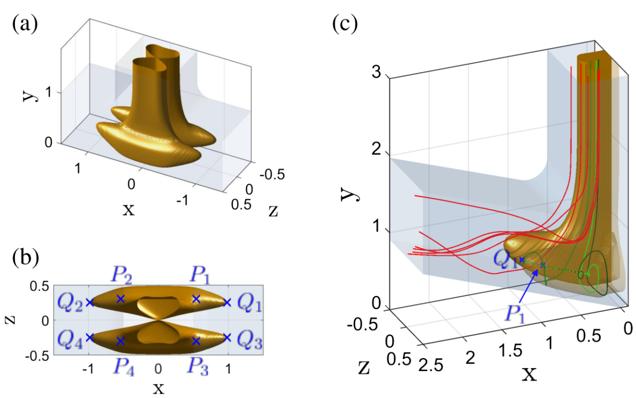

FIG. 2. Primary trapping regions (TRs, colored yellow) in the T- and V-junction flows for $\varepsilon = 0.05$. This value of ε corresponds to, e.g., hollow glass beads ($\rho = 0.15$) with $\beta = 2.3078$, $\tau = 0.0382$, and St = 0.0588 used in experiments [4], or gas bubbles ($\rho = 10^{-3}$) with $\beta = 2.994$, $\tau = 0.0251$, and St = 0.0501. Blue crosses mark the fixed points $P_{1,2,3,4}$ and $Q_{1,2,3,4}$. (a) T junction at Re = 320 (beads with $a = 2.9 \times 10^{-2}$, bubbles with $a = 2.7 \times 10^{-2}$). (b) T junction viewed from the top. (c) V junction at Re = 230, with representative particle trajectories (beads with $a = 3.4 \times 10^{-2}$, bubbles with $a = 3.1 \times 10^{-2}$). The boundary of the TR separates trajectories that exit through the outlet (red) and trajectories that remain inside the TR and spiral onto the extended vortex axis (green).

These TRs intersect with the inlet cross section, allowing for incoming particles to be trapped.

Just as the vortex breakdown regions (cf. the Supplemental Material [5], Fig. S1, shown in green) that were used to predict particle capture previously [4], the TRs end at fixed points $Q_{1,2}$ and $Q_{3,4}$ [Fig. 2(b)]. Comparing Fig. S1 of the Supplemental Material [5] to Fig. 2(b), however, we observe that the TRs occupy a much larger part of the domain than the vortex breakdown regions. Each TR has a shape resembling an "anchor" and contains one vortex in each arm. We are unaware of prior descriptions of such regions in the literature.

For hollow glass beads ($\varepsilon = 0.05$) in the V-junction flow at $\mathrm{Re} = 230$, we find similar TRs [Fig. 2(c)]. Their boundaries impact the shape of nearby trajectories: Passing trajectories are deformed by the TRs before exiting the junction. Inside the TRs, particles spiral away from the surface and quickly converge to a one-dimensional manifold (cf. the Supplemental Material [5], Fig. S1). This fast attraction within the TRs (occurring within time $t \lesssim 2$) explains why previous dye experiments (cf. Fig. S8 in Ref. [3]) did not reveal these regions. Despite their significant impact on particle motion, the anchor-shaped boundaries of TRs are effectively invisible surfaces.

For the V-junction flow at $\mathrm{Re} = 230$, we explore the parameter dependence of the TRs by considering different values of ε that correspond to the full range of particle sizes in the experiments with gas bubbles (cf. Ref. [4]). For the smallest bubbles ($a = 5.0 \times 10^{-4}$, $\mathrm{St} \approx \varepsilon = 1.3 \times 10^{-5}$), we do not observe trapping. For slightly larger bubbles [$a = 6.1 \times 10^{-3}$, $\mathrm{St} \approx \varepsilon = 1.9 \times 10^{-3}$; cf. Fig. 3(a)], we find two well-separated TRs that reach into the inlet arm. However, since their intersection with the inlet is small [Fig. 3(a)], it is unlikely that these TRs will capture bubbles entering at random inlet positions.

Increasing the particle size further [$a = 1.1 \times 10^{-2}$, $\mathrm{St} \approx \varepsilon = 6.6 \times 10^{-3}$; cf. Fig. 3(b)], the TRs grow and their separation decreases. For $\mathrm{St} \approx \varepsilon_M = 0.0161$, the TRs are so close to each other that, within the inlet cross section, their minimum distance is equal to the particle diameter [$a = 1.8 \times 10^{-2}$; cf. Fig. 3(c)]. For consistency with our model, which represents finite-size particles as points, we view this as a merger of the separate TRs into a single, larger TR. The critical value $\varepsilon_M = 0.0161$, therefore, defines a topological transition for the trapping of gas bubbles in water for the V-junction flow at $\mathrm{Re} = 230$.

For the largest bubbles [$a = 2.5 \times 10^{-2}$, $\mathrm{St} \approx \varepsilon = 0.0319$; cf. Fig. 3(d)], the two TRs touch over a large distance and form a single TR occupying a large portion of the inlet cross section [cf. Fig. 3(d)]. Overall, the TR is so large that it touches the domain boundary over significant areas. Since the Stokes drag law is not valid close to walls, our model is inconclusive in these regions. Thus, the size of the TR shown in Figs. 3(c) and 3(d) is likely an overestimate compared to the actual experimental dynamics [4].

Given that ε is the only parameter in Eq. (1), within our approximation, the TRs for hollow glass beads are identical to Fig. 3. The critical value ε_M for the merger of the two TRs, however, depends on the radius a of the particles at a given ε and hence, by Eq. (2), ε_M depends on the choice of particle. Within our numerical accuracy, however, we find that $\varepsilon_M = 0.0161$ for beads is approximately the same as for bubbles.

For the T junction, for $\varepsilon > \varepsilon_M$, we find that the TRs touch along the line defined by $x = 0$, $z = 0$ [cf. Fig. 2(b)]. The numerical values are $\varepsilon_M = 0.0226$ for gas bubbles and $\varepsilon_M = 0.0230$ for hollow glass beads in water at $\mathrm{Re} = 320$. Even for $\varepsilon \gg \varepsilon_M$, however, the TRs continue to touch only along that line. Unlike for the V junction, therefore, we regard the TRs as remaining separate here. Albeit the TRs remain technically unmerged for T junctions, we still refer to the development of the intersection between these two TRs along the line $x = 0$, $z = 0$ as a transition. Indeed, experimental or numerical observations of these regions via particle trajectories will suggest a full merger because the particle size exceeds the remaining small distances between them.

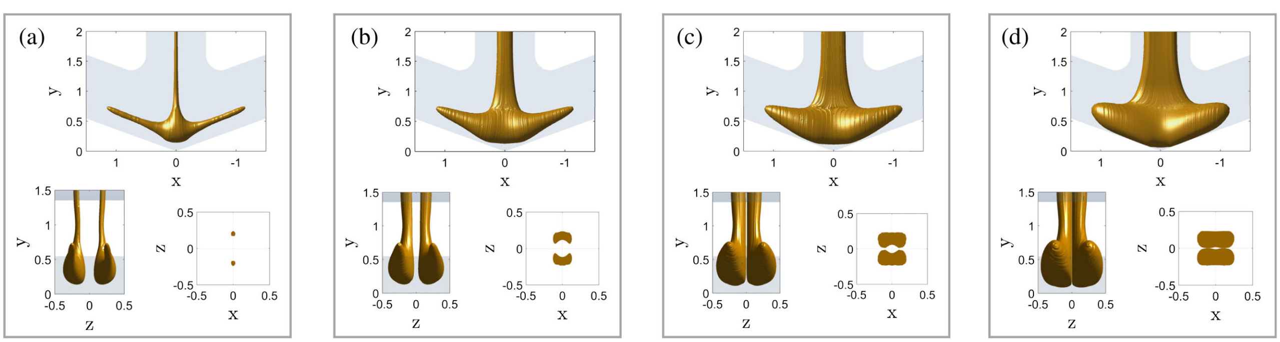

FIG. 3. Trapping regions in the V-junction flow at $\mathrm{Re} = 230$ for different Stokes numbers St representing the range of experimentally observed bubble sizes (between $a = 5.0 \times 10^{-4}$ and $a = 2.5 \times 10^{-2}$ [4]). (a) $\mathrm{St} \approx \varepsilon = 1.9 \times 10^{-3}$ ($a = 6.0 \times 10^{-3}$). (b) $\mathrm{St} \approx \varepsilon = 6.6 \times 10^{-3}$ ($a = 1.1 \times 10^{-2}$). (c) Critical case, merger of TRs: $\mathrm{St} \approx \varepsilon = \varepsilon_M = 0.0161$ ($a = 1.8 \times 10^{-2}$). (d) $\mathrm{St} \approx \varepsilon = 0.0319$ ($a = 2.5 \times 10^{-2}$). (Bottom-left panels) $z - y$ views showing that, below the critical value $\mathrm{St} \approx \varepsilon_M = 0.0161$, the TRs are well separated. (Bottom-right panels) Intersections of the inlet cross section ($y = 3$) with the TRs.

Because of the symmetry of the fixed points $P_{1,2,3,4}$, the stability of P_1 determines the existence of the TRs. By Eq. (1), we monitor the signs of the real parts of the eigenvalues of $\nabla \boldsymbol{v}(\boldsymbol{x})|_{\boldsymbol{x}=P_1}$: In both the T- and V-junction flows, for $\varepsilon < \varepsilon_C$, the eigenvalue for the eigenvector aligned with the vortex has positive real part, causing instability and preventing trapping. For $\varepsilon > \varepsilon_C$, the eigenvalue becomes negative, turning P_1 into an attracting fixed point and leading to trapping. The numerical values are $\varepsilon_C = 0.001\,23$ for the T junction and $\varepsilon_C = 0.001\,83$ for the V junction. In contrast to ε_M, in our approximation the value of ε_C does not depend on the particle type.

By Eq. (2), the condition $\varepsilon = \mathrm{St}(1-\rho) > \varepsilon_C$ defines a parameter region of ρ, St, β, and a where particle capture in the T and V junctions occurs [Figs. 4(a) and 4(b)]. Since the values of ε_C for the T and V junctions are similar, these regions are almost identical for both cases. Overall, Fig. 4 predicts that, for a high enough St, any light particle ($\rho < 1$) becomes captured. This result differs from previous work [3] which used a force balance of simplified fluid-particle forces and estimated that capture is possible only for $\rho \lesssim 0.7$. While recent experiments [4] did not explore the capture limit on ρ, they did show capture at $\rho = 0.72$. As our model disregards flow distortions due to other particles, we expect the actual capture limit to be $1.0 \geq \rho \geq 0.72$ in the presence of such effects.

In addition, from $\varepsilon = \mathrm{St}(1-\rho)$, we obtain a lower limit on St: For $\mathrm{St} < \varepsilon_C$, even the lowest density particles ($\rho \to 0$) are not captured. In particular, according to our model, we do not expect capture for some of the smallest bubbles and hollow glass beads appearing in the experiments [4] (T junction, $5.0 \times 10^{-4} \lesssim a \lesssim 4.5 \times 10^{-3}$; V junction, $5.0 \times 10^{-4} \lesssim a \lesssim 6.5 \times 10^{-3}$). For the V junction [Fig. 4(b)], the parameter region for capture is further divided into two subregions where trapping occurs either in two separate TRs [cf. Figs. 3(a) and 3(b)] or, for $\varepsilon > \varepsilon_M$, in a single TR [cf. Fig. 3(d)]. As noted, however, the value of ε_M has a minor dependence on the particle type.

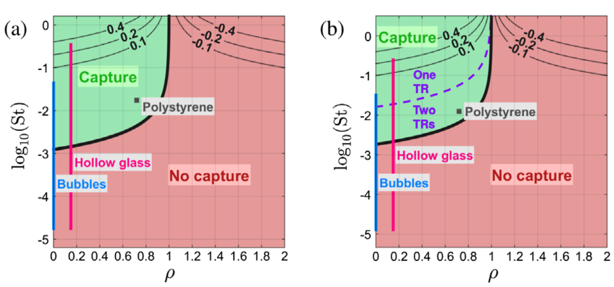

FIG. 4. Parameter regions of St and ρ where capture occurs. Vertical lines and squares mark St and ρ values of particles from the experiments in Ref. [4]. Gas bubbles, blue; hollow glass beads, magenta; and polystyrene beads, gray. Thin black curves are level sets of ε [see Eq. (2)], indicating parameter regions where we expect that Eq. (1) ceases to be valid. (a) T junction at Re = 320. (b) V junction at Re = 230. Capture occurs either in two TRs, or, for $\varepsilon > \varepsilon_M = 0.016$, in a single TR.

To our knowledge, the anchor-shaped TRs discovered in this Letter have not been recognized before. They are much larger than the recirculation regions previously proposed to predict particle capture in branching junctions [4]. For applications where throughput of particles is crucial, it is important to be aware of these transport barriers for the particles.

Available limits on Re and the junction angle (cf. Fig. 5 in Ref. [4]) identify flow regimes where capture occurs. Considering the great similarities between our results for the T junction at Re = 320 and the V junction at Re = 230, we believe that the mechanism we document is universal within this class of flows. Our estimates on the ranges of St and ρ leading to trapping (Fig. 4) hence complement the known bounds on the fluid parameters.

Particle capture has been documented for unsteady flows through branching junctions of different angles than are considered here [3,4]. In the Supplemental Material [5], we therefore introduce a Lagrangian Q criterion capable of detecting TRs in flows with arbitrary time dependence. This criterion shows that for Eq. (1), accumulation of particles with $\rho < 1$ occurs only while they move in vortical regions defined by the Q criterion [13]. Earlier work suggested that regions of negative Eulerian divergence in planar steady flow of inertial particles indicate areas of particle accumulation [9,10]. However, in fact, these regions imply only the shrinkage of the particle cloud volume. By contrast, our Lagrangian Q criterion identifies lower-dimensional, finite-time attractors that extremize the backward-integrated Lagrangian divergence.

With the TRs directly linked to the presence of vortices, we expect that similar regions exist in other channel flows (cf. e.g., Ref. [14]). Our analysis provides a template for investigations of the 3D geometry of such TRs. This template is robust under small perturbations, given the structural stability of slow manifolds and finite-time attractors used in its construction [15–17]. Our conclusions assume no interaction among particles and the fluid, which no longer holds once particles accumulate on their finite-time attractor. As this effect is secondary and localized to the vicinity of the attractors, we expect limited deformation relative to the identified TRs.

One important application of the detailed detection of TRs is the control of particle trapping and, thus, the design of microfluidic devices. Recent work [18], e.g., showed that the vortical flow structures in the 70° V junction flow at Re = 230 enable the rapid, flow-driven fusion of lipid vesicles. Producing large quantities of giant unilamellar vesicles requires combining V junctions into larger devices. We thus expect that computing the TRs will assist in identifying efficient channel configurations for trapping particles.

The Department of Energy will provide public access to these results of federally sponsored research in accordance with the DOE Public Access Plan [19].

We thank Sophie Calabretto and Sascha Hilgenfeldt for the helpful discussions. This work has been partially supported by the Turbulent Superstructures Program of the German National Science Foundation (DFG). The Laboratory Directed Research and Development Program of Oak Ridge National Laboratory is managed by UT-Battelle, LLC, under Contract No. DE-AC05-00OR22725 for the U.S. Department of Energy. The U.S. Government retains, and the publisher, by accepting the article for publication, acknowledges that the U.S. Government retains, a nonexclusive, paid-up, irrevocable, worldwide license to publish or reproduce the published form of this manuscript or allows others to do so for U.S. Government purposes.

[*]georgehaller@ethz.ch

[1] B. E. Larock, R. W. Jeppson, and G. Z. Watters, *Hydraulics of Pipeline Systems* (CRC Press, Boca Raton, 1999).

[2] T. Karino, H. L. Goldsmith, M. Motomiya, S. Mabuchi, and Y. Sohara, Ann. N.Y. Acad. Sci. **516**, 422 (1987).

[3] D. Vigolo, S. Radl, and H. A. Stone, Proc. Natl. Acad. Sci. U.S.A. **111**, 4770 (2014).

[4] J. T. Ault, A. Fani, K. K. Chen, S. Shin, F. Gallaire, and H. A. Stone, Phys. Rev. Lett. **117**, 084501 (2016).

[5] See Supplemental Material at http://link.aps.org/supplemental/10.1103/PhysRevLett.121.054502 for an experimental video, additional simulation results, and a derivation of the Lagrangian Q criterion.

[6] K. K. Chen, C. W. Rowley, and H. A. Stone, Phys. Fluids **27**, 034107 (2015).

[7] K. K. Chen, C. W. Rowley, and H. A. Stone, J. Fluid Mech. **815**, 257 (2017).

[8] M. R. Maxey, J. Fluid Mech. **174**, 441 (1987).

[9] K.-K. Tio, J. C. Lasheras, A. M. Gañán-Calvo, and A. Linan, in *Advances in Turbulence IV*, edited by F. T. M. Nieuwstadt (Springer, New York, 1993), p. 285.

[10] K.-K. Tio, A. Liñán, J. C. Lasheras, and A. M. Gañán-Calvo, J. Fluid Mech. **254**, 671 (1993).

[11] G. Haller and T. Sapsis, Physica (Amsterdam) **237D**, 573 (2008).

[12] H. G. Weller, G. Tabor, H. Jasak, and C. Fureby, Comput. Phys. **12**, 620 (1998).

[13] J. C. Hunt, A. A. Wray, and P. Moin, Center for Turbulence Research, Stanford University Report No. CTR-S88, 1988.

[14] R. Thameem, B. Rallabandi, and S. Hilgenfeldt, Biomicrofluidics **10**, 014124 (2016).

[15] G. D. Birkhoff, Acta Math. **50**, 359 (1927).

[16] J. Palis and S. Smale, in *The Collected Papers of Stephen Smale: Volume 2*, edited by F. Cucker and R. S. C. Wong (World Scientific, Singapore, 2000), p. 739.

[17] J. Guckenheimer and P. Holmes, *Nonlinear Oscillations, Dynamical Systems, and Bifurcations of Vector Fields*, Vol. 42 (Springer Science+Business Media, New York, 2013).

[18] S. Shin, J. T. Ault, and H. A. Stone, Langmuir **31**, 7178 (2015).

[19] See http://energy.gov/downloads/doe-public-access-plan.